PNAS RESEARCH ARTICLE | GENETICS OPEN ACCESS

Oncogenic IDH1^{mut} drives robust loss of histone acetylation and increases chromatin heterogeneity

Noa Furth[a], Niv Cohen[a], Avishay Spitzer[b,c,d], Tomer-Meir Salame[e], Bareket Dassa[f], Tevie Mehlman[g], Alexander Brandis[g], Arieh Moussaieff[h], Dinorah Friedmann-Morvinski[i], Maria G. Castro[j], Jerome Fortin[k], Mario L. Suvà[l,m], Itay Tirosh[b], Ayelet Erez[b], Guy Ron[n], and Efrat Shema[a,1]

Affiliations are included on p. 10.

Edited by Anjana Rao, La Jolla Institute for Immunology, La Jolla, CA; received February 23, 2024; accepted November 15, 2024

Malignant gliomas are heterogeneous tumors, mostly incurable, arising in the central nervous system (CNS) driven by genetic, epigenetic, and metabolic aberrations. Mutations in isocitrate dehydrogenase (IDH1/2^{mut}) enzymes are predominantly found in low-grade gliomas and secondary high-grade gliomas, with IDH1 mutations being more prevalent. Mutant-IDH1/2 confers a gain-of-function activity that favors the conversion of a-ketoglutarate (α-KG) to the oncometabolite 2-hydroxyglutarate (2-HG), resulting in an aberrant hypermethylation phenotype. Yet, the complete depiction of the epigenetic alterations in IDH^{mut} cells has not been thoroughly explored. Here, we applied an unbiased approach, leveraging epigenetic-focused cytometry by time-of-flight (CyTOF) analysis, to systematically profile the effect of mutant-IDH1 expression on a broad panel of histone modifications at single-cell resolution. This analysis revealed extensive remodeling of chromatin patterns by mutant-IDH1, with the most prominent being deregulation of histone acetylation marks. The loss of histone acetylation occurs rapidly following mutant-IDH1 induction and affects acetylation patterns over enhancers and intergenic regions. Notably, the changes in acetylation are not predominantly driven by 2-HG, can be rescued by pharmacological inhibition of mutant-IDH1, and reversed by acetate supplementations. Furthermore, cells expressing mutant-IDH1 show higher epigenetic and transcriptional heterogeneity and upregulation of oncogenes such as KRAS and MYC, highlighting its tumorigenic potential. Our study underscores the tight interaction between chromatin and metabolism dysregulation in glioma and highlights epigenetic and oncogenic pathways affected by mutant-IDH1-driven metabolic rewiring.

chromatin | mutant-IDH1 | oncometabolite | epigenetics | CyTOF

Cell-type-specific chromatin organization, crucial for establishing cellular identity, is achieved by orchestrated and tightly regulated deposition of DNA and histone modifications. The core histones are extensively and dynamically modified by covalent attachment of various chemical groups, such as acetylation and methylation of different lysine residues (1, 2). Chromatin alterations are highly frequent across human cancers, with many tumors harboring mutations in chromatin modifiers (3–6). This is exemplified in malignant gliomas, aggressive tumors arising in the central nervous system (CNS), in which chromatin-related pathways are either directly mutated or indirectly deregulated, suggesting epigenetic reprogramming as a major driver of these tumors (7).

Isocitrate dehydrogenase (IDH1/2) enzymes are frequently mutated in adult gliomas, and their mutation status is currently used for CNS tumor classification (8, 9). IDH^{mut} gliomas share clinical characteristics, such as low histological grade, age of onset, and anatomical location (7). While having a better prognosis than IDH^{wt} gliomas, these tumors grow continuously, infiltrate normal brain tissue, and eventually become aggressive tumors with accelerated tumor growth and neovascularization (9–11). The mutations, found predominantly in the IDH1 (R132H) enzyme, and less frequently in IDH2 (R172H), are heterozygous and considered early somatic events in these tumors (9, 12, 13). WT IDH enzymes convert the TCA metabolite isocitrate into alpha-ketoglutarate (αKG) while generating NADPH (14). The cancer-associated mutations in IDH alter the catalytic pocket of the enzymes, causing further reduction of αKG into the oncometabolite 2-Hydroxyglutarate (2-HG) (15, 16). This results in more than a 100-fold increase in 2-HG levels in glioma cells expressing mutant-IDH. 2-HG acts as a competitive inhibitor of enzymes that rely on αKG as a cofactor, spanning various cellular functions (17). Among these are aKG-dependent demethylases of histones and DNA, whose inhibition by mutant-IDH results in perturbed chromatin architecture and function (7). IDH^{mut} cells exhibit higher levels of DNA and histone methylation, which have been associated with differentiation block and can facilitate tumorigenesis (18–20).

Significance

Mutations in the metabolic enzyme isocitrate dehydrogenase (IDH1) are frequent and considered early events in a subset of adult gliomas. The mutant IDH1 enzyme changes functionally, favoring the production of the oncometabolite 2-hydroxyglutarate, and alters metabolic and epigenetic pathways. However, a comprehensive understanding of the epigenetic landscape in IDH1^{mut} cells and how it contributes to tumorigenesis is lacking. This study presents a high-dimensional single-cell analysis of chromatin alterations driven by mutant-IDH1. Our analysis reveals extensive remodeling of chromatin patterns, highlighting a rapid decrease in histone acetylation marks and increased epigenetic heterogeneity. These changes in histone acetylation, affecting enhancer patterns, are strongly associated with the metabolic abnormalities of IDH1^{mut} cells, underscoring the interplay between chromatin and metabolism dysregulation in glioma.

The authors declare no competing interest.

This article is a PNAS Direct Submission.

[1]To whom correspondence may be addressed. Email: efrat.shema@weizmann.ac.il.

This article contains supporting information online at https://www.pnas.org/lookup/suppl/doi:10.1073/pnas.2403862122/-/DCSupplemental.

Published December 30, 2024.

In addition, IDH^{mut} cells undergo massive metabolic reprogramming (21–23). Recent studies revealed a tight connection between the metabolic state of cells and the epigenetic machinery, often hijacked in different ways during tumorigenesis (24–26). Thus, the changes in histone and DNA methylation documented to follow the 2-HG elevation may not be the only metabolic alteration that reprograms the chromatin landscape in IDH^{mut} gliomas. We recently adapted CyTOF to profile a wide array of histone modifications in single cells, demonstrating the power of such analysis in revealing chromatin alterations in cancer (27). Here, we leveraged this epigenetic-focused CyTOF methodology to systematically profile the effects of mutant-IDH1 expression on the chromatin states of cells. We revealed dynamic and extensive remodeling of chromatin, mainly affecting histone acetylation and altering the enhancer landscape of cells, rather than histone methylation. Finally, the single-cell analysis revealed higher epigenetic diversity within cells expressing mutant-IDH1, leading to increased epigenetic heterogeneity, providing a potential selective advantage for these cells.

Results

Mutant-IDH1 Elicits Global Alterations to Histone Methylation and Acetylation Marks. The IDH1-R132H mutation is considered an early event in glioma development and thus is thought to play roles in tumor initiation (13). To study early epigenetic changes driven by mutant-IDH1, we expressed FLAG-tagged IDH1-R132H in immortalized human astrocytes (IHA, Fig. 1*A* and *SI Appendix*, Fig. S1*A*). We verified that mutant-IDH1 expression levels were comparable to those detected in a previously published system of IDH^{mut} glioma, as well as glioma cells endogenously expressing the mutant protein (*SI Appendix*, Fig. S1*B*). High levels of the oncometabolite 2-HG were detected following the induction of mutant-IDH1 by doxycycline (Fig. 1*B*). To systematically explore the extent and dynamics of chromatin alterations mediated by mutant-IDH1 expression, we utilized our recently developed epigenetic-CyTOF method to profile an extensive array of histone modifications (27). Our panel consists of metal-conjugated antibodies targeting multiple histone modifications and chromatin regulators, core histone proteins, and the mutant-IDH1 protein (Fig. 1*C*). Dimensionality reduction using uniform manifold approximation and projection (UMAP) analysis of IHA cells expressing IDH1-R132H revealed consistent alterations in various epigenetic marks. This resulted in a gradual shift of the center of distribution of cells expressing the mutant enzyme for 2, 4, and 7 d (*SI Appendix*, Fig. S1 *C–E*). The levels of multiple chromatin modifications were altered by expression of mutant-IDH1, with different patterns observed for different modifications (Fig. 1*D* and *SI Appendix*, Fig. S2). To explore the dynamics of these alterations, we calculated the trajectory of change for each modification following induction of mutant-IDH1 and plotted the correlations between the trajectories of all modifications, so that modifications that showed a similar trajectory of change are clustered together (Fig. 1*E*). This analysis revealed two distinct patterns; most histone methylation marks, with the exception of H3K27me3, increased following mutant-IDH1 induction. On the contrary, all histone acetylation marks that we measured robustly decreased. The histone hypermethylation phenotype of IDH1-R132H cells has been reported by several studies, mostly focusing on late passaged cells with prolonged mutant-IDH1 expression (18, 28, 29); our data revealed that the increase in some methylation marks, such as H3K9me3 and H3K4me3, could be seen as early as 2 to 4 d after induction. In addition, our analysis revealed marked and rapid decrease in both H3 and H4 acetylation marks (H3K27ac, H3K64ac, H3K9ac, and H4K16ac) induced by expression of IDH1-R132H, in line with a previous bulk mass spectrometry analysis (30). To confirm that these epigenetic alterations are indeed specific to expression of the mutant enzyme and are not caused by IDH1 over expression, we compared astrocytes induced to express either WT or mutant IDH1 (*SI Appendix*, Fig. S3*A*). Notably, cells expressing mutant-IDH1 showed reduced levels of histone acetylation marks, along with increase in methylation marks, also when compared to cells ectopically expressing WT IDH1 (*SI Appendix*, Fig. S3 *B* and *C*). The reduction in histone acetylation marks is seen early after induction of mutant-IDH1, co-occurring, or even preceding the increase in histone methylation, and was also confirmed by western blot (Fig. 1 *F* and *G*). Overall, our unbiased analysis revealed multiple epigenetic changes occurring following mutant-IDH1 induction, with both methylation and acetylation marks being significantly altered.

Loss of Histone Acetylation is seen Across Multiple Systems and can be Reverted by Pharmacological Inhibition of Mutant-IDH1. To examine whether this loss of histone acetylation is unique to the context of astrocytes or represents a general effect of mutant-IDH1 expression, we induced the mutant enzyme in two highly diverse systems: The HEK293 cells and the glioblastoma (GBM) cells (MGG18) cells, engineered to express mutant-IDH1 in a doxycycline-dependent manner. Western blot analysis revealed that even in HEK293 cells, which arise from human embryonic kidney, induction of mutant-IDH1 resulted in loss of acetylation of H3 and H4 (Fig. 2*A*). CyTOF analysis of the MGG18 cells, expressing mutant-IDH1 for a prolonged period (over 2 mo), thus modeling long-term adaptation to mutant-IDH1 expression, also revealed loss of all measured histone acetylation marks compared to noninduced cells (Fig. 2*B* and *SI Appendix*, Fig. S3*D*). Finally, we also observed histone H3 and H4 hypoacetylation on multiple lysine residues in mutant-IDH1 cells derived from a mouse glioma model, in addition to the reduction in H3K27ac recently reported by Garrett et al. (31) (*SI Appendix*, Fig. S3*E*).

Pharmacological inhibition of mutant-IDH1 with AGI5198 reverted the epigenetic changes induced by the mutant protein, resulting in a reduction in histone methylation and an increase in histone acetylation levels (Fig. 2*C*). Similarly, inhibition of mutant-IDH1 by either AGI5198 or Vorasidenib (AG-881) increased histone acetylation levels in both the human GBM cells MGG119, endogenously expressing $IDH1^{R132H}$, and mouse glioma cells driven by endogenous $Idh1^{R132H}$ (Fig. 2 *D* and *E*) (32). These results further verify the direct role of mutant-IDH1 protein in mediating these epigenetic changes. Of note, Vorasidenib was shown to significantly improve progression-free survival in recurrent IDH mutant grade 2 glioma patients [INDIGO trial, NCT04164901 (33)], leading to drug-induced lineage differentiation (34). The differentiation phenotype might be linked to the robust epigenetic changes mediated by this drug.

We next compared the early epigenetic changes induced by mutant-IDH to the effect of supplementing the cells with 2-HG. To that end, astrocytes were treated with a cell-permeable form of 2-HG (octyl-2HG) and analyzed with the epigenetic CyTOF panel. 2-HG induced mild epigenetic alterations which were mostly distinct from the IDH1-mediated epigenetic changes. As expected, several histone methylation marks, such as H3K9me3 and H3K36me2, were higher in 2-HG treated cells. Interestingly, while the levels of H4K16ac were reduced, we did not observe an overall reduction in histone acetylation as seen following mutant-IDH1 induction (Fig. 2*F* and *SI Appendix*, Fig. S4). Thus,

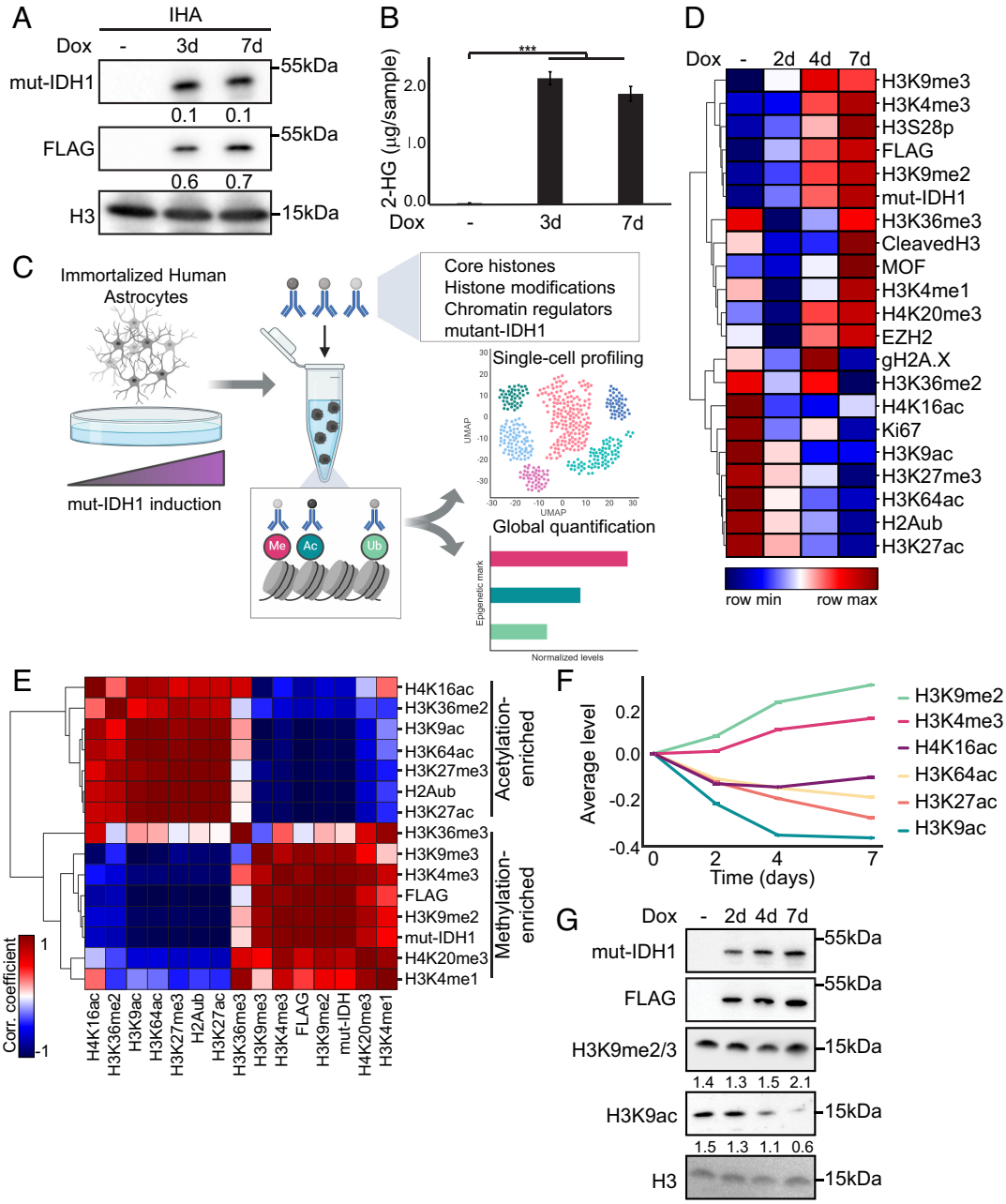

Fig. 1. Mutant-IDH1 elicits global changes in chromatin patterns, with early loss of histone acetylation. (*A*) IHA were treated with doxycycline for the indicated time points to induce expression of FLAG-tagged IDH1-R132H. Western blot of total cell lysate with the indicated antibodies is shown. Signal intensity was normalized to H3 signal and indicated below each blot. (*B*) Quantification of cellular 2-HG levels in IHA expressing IDH1-R132H for the indicated time points, as measured by LC–MS/MS. Mean ± SE of three replicates are shown. *** *P*-value < 0.001; two-sided *t* test. (*C–F*) IHA were induced to express IDH1-R132H for 2, 4, and 7 d, following CyTOF analysis. (*C*) Scheme of CyTOF experimental setup and analysis. Cells were fixed and incubated with a panel of chromatin-related antibodies, along with antibodies targeting core histones and the ectopically expressed IDH1-R132H. For each cell, quantification of each feature is obtained, and normalized to the levels of the core histone (*Methods Summary*). The illustration was created with BioRender.com. (*D*) Heatmap of the mean levels of the indicated features in each of the IHA samples as measured by CyTOF. Rows are standardized and clustered; red and blue denote high and low levels of the modifications, respectively. (*E*) Heatmap of the correlations between the means of distributions of the modifications at the different time points, indicating similarity in the trajectories of change of each modification in response to mutant-IDH1 induction. Red denotes high degree of correlation between modifications that varied together. Clustering shows distinct trends with methylation marks increasing and acetylation marks decreasing following mutant-IDH1 induction. (*F*) Mean ± SE calculated by bootstrapping, for the indicated histone mark in the indicated time point, are shown. (*G*) Western blot analysis of the samples described in *F* with the indicated antibodies. Signal intensity was normalized to H3 signal and indicated below each blot. CyTOF panel composition used for each experiment is described in *SI Appendix*, Table S2.

increased levels of 2-HG following mutant-IDH1 expression contribute to histone methylation but cannot solely explain the decrease in histone acetylation marks. Overall, our results suggest that mutant IDH1-dependent loss of histone acetylation is a broad and robust phenomenon seen in multiple experimental models and is not solely manifested by the increase in 2-HG levels.

Mutant-IDH1 Alters Acetyl-CoA Metabolism, which can be Rescued by Acetate Supplement. We reasoned that mutant-IDH1 induction may deregulate the levels of additional metabolites that can affect the chromatin state (35). Previous studies have shown that histone acetylation is tightly linked to cellular levels of acetyl-CoA and acetate (24, 36–38). Thus, we hypothesized

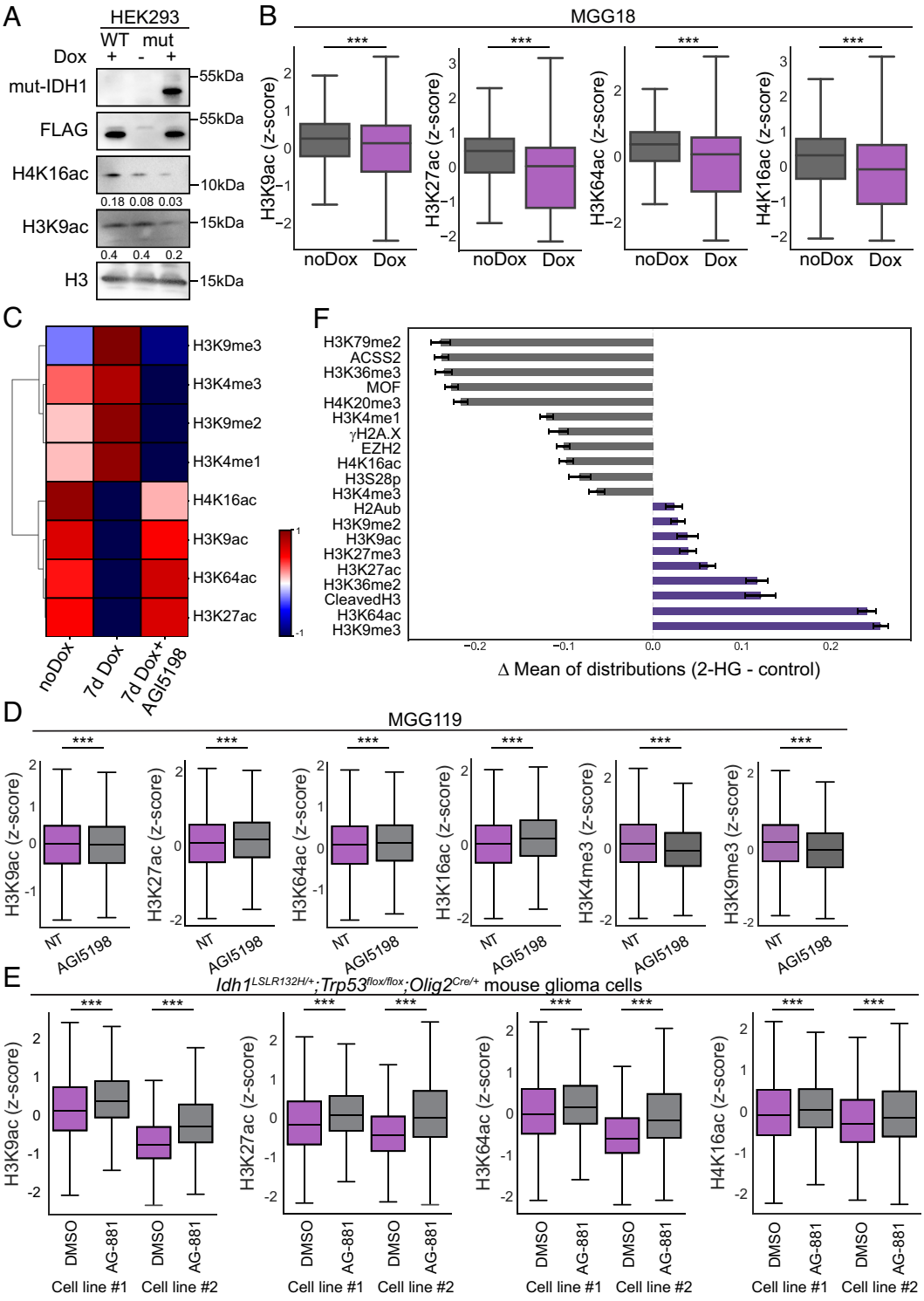

Fig. 2. Reversal of histone acetylation loss by pharmacological inhibition of mutant-IDH1. (*A*) HEK293 cells were induced to express either WT or IDH1-R132H for 7 d, and analyzed by western blot with the indicated antibodies. Signal intensity was normalized to H3 signal and indicated below each blot. (*B*) MGG18 cells were induced to express IDH1-R132H for over 2 mo and analyzed by CyTOF, in comparison to cells not treated with doxycycline. Mutant-IDH1 cells show lower levels of acetylation marks. Box plots depict CyTOF measurements of the indicated modifications; ***P-value < 0.001. (*C*) IHA were induced to express mutant-IDH1 for 7 d. 2 d after initiation of induction, cells were treated with 5 μM of AGI5198 for a total of 5 d. Heatmap of the mean levels of the indicated features in each of the samples as measured by CyTOF is shown. Rows are standardized and clustered. (*D*) MGG119 cells (human GBM endogenously expressing $IDH1^{R132H}$) were treated with 5 μM of AGI5198 for 6 d prior to CyTOF analysis. Inhibition of mutant-IDH1 results in an increase in acetylation marks. Box plots depict CyTOF measurements of the indicated modifications; ***P-value < 0.001. (*E*) Histone acetylation levels were measured by CyTOF in two pairs of treated (AG-881, 1 μM) and untreated mouse glioma cells ($Idh1^{LSL\text{-}R132H}$;$Trp53^{flox/flox}$;$Olig2^{Cre}$) (32). Box plots depict CyTOF measurements of the indicated modifications; ***P-value < 0.001. (*F*) IHA were treated with 0.5 mM octyl-2HG for 7 d and analyzed by CyTOF. Shown are the mean differences between control and 2-HG treated cells for the indicated feature. The mean values for the control were subtracted from 2-HG treated cells. Error bars represent SEM, calculated by bootstrapping. Features that were increased upon 2-HG treatment are marked in purple. Supplement of 2-HG results in common and distinct changes as compared to mutant-IDH1 expression. CyTOF panel composition used for each experiment is described in *SI Appendix*, Table S2. All P-values were calculated by Welch's t test.

that metabolic rewiring of mutant-IDH1 cells may shift the use of these metabolites, resulting in reduced histone acetylation. Supporting this hypothesis, we found that the expression patterns of several genes that are part of different metabolic pathways related to acetyl-CoA homeostasis were altered upon induction of mutant-IDH1 (Fig. 3 *A* and *B* and *SI Appendix*, Fig. S5*A* and Table S3). Interestingly, analysis of expression data from human WT or IDH1^{mut} gliomas revealed a significant reduction in three of these key metabolic genes, in accordance with the changes observed in the inducible system (Fig. 3*C*).

Next, we set to directly measure the levels of cellular acetyl-CoA over multiple time points following mutant IDH1 induction. As early as 24 h after induction, we observed a reduction in acetyl-CoA levels, supporting the notion that expression of mutant-IDH1 rewires the metabolic state of the cells, limiting acetyl-CoA availability (Fig. 3*D* and *SI Appendix*, Fig. S5*B*). Moreover, inhibition of mutant-IDH1 increased acetyl-CoA levels in cells induced to express the mutant protein (Fig. 3*E* and *SI Appendix*, Fig. S5*C*). In line with this metabolic rewiring and a previous report, mutant-IDH1 cells were sensitive to HDAC inhibition, potentially due to the inability of cells to increase the acetyl pool upon treatment with these inhibitors (Fig. 3*F*) (31).

To further explore the possibility that the reduction in histone acetylation is due to a shortage in acetate-driven metabolites, we supplemented the cells with acetate, which restored the deposition of acetyl groups on H3 and H4 histones (Fig. 3 *G* and *H*). Of note, mutant-IDH1 cells showed a larger fold increase (acetate-treated vs. control cells) than cells not expressing the mutant enzyme. This supports the notion that the histone acetylation machinery in these cells is intact, and once provided with a substrate, the cells can restore acetylation levels. Taken together, our data suggest that the loss of histone acetylation driven by mutant-IDH1 is caused by metabolic rewiring and changes in the cellular availability of acetyl-CoA and acetate.

To further explore the relevance of our findings to human IDH1-mutant gliomas, we obtained and analyzed two clinically relevant datasets: 1) oligodendroglioma patients treated with mutant-IDH inhibitors, from a perioperative phase 1 trial (NCT03343197); and 2) single-cell RNA-seq data from eight oligodendroglioma samples, two of which were treated with mutant-IDH inhibitors (34, 40–42). In agreement with our experimental systems, we found that mutant-IDH inhibition in patients diagnosed with IDH^{mut} gliomas altered the expression of acetyl-CoA-related metabolic genes, supporting a direct role for mutant-IDH1 in rewiring of this metabolic hub (Fig. 3*I* and *SI Appendix*, Fig. S5*D*). For example, while Pyruvate Dehydrogenase Kinase (PDK) and ACSS (Acyl-CoA Synthetase) family members were down-regulated upon induction of mutant-IDH1, its inhibition resulted in increased expression of these genes. Similarly, the expression levels of ACLY increased in mutant-IDH1 cells, while reduced in tumors treated with the inhibitor. Interestingly, while CPT1A increased upon mutant-IDH1 induction in our IHA cells, CPT1C mildly decreased. In the single-cell dataset, these two genes showed opposite patterns, potentially due to context-dependent regulation of these two family members. Of note, while the dominantly expressed family member in the IHA cells was CPT1A, human tumors showed higher expression of CPT1C, in agreement with mutant-IDH1 activating the transcription of both genes (Fig. 3*B* and *SI Appendix*, Fig. S5*D*). These results suggest that mutant-IDH1 alters metabolic pathways related to acetyl CoA homeostasis in our model system and in human tumors.

Finally, we examined whether the growth of mutant-IDH1 cells may also be influenced by external acetate levels, potentially revealing a metabolic dependency of these cells. MGG18 cells, expressing mutant-IDH1, showed reduced growth rates when cultured with limited amounts (0.05 to 0.1%) of the serum-free supplement B-27, as expected (Fig. 3*J*). Importantly, supplementing this limited media with acetate increased the growth rates, suggesting that the availability of external acetate supports proliferation of these cancer cells (Fig. 3*K*).

Mutant-IDH1 Expression Alters the Enhancer Landscape to Promote Oncogenic Transcription. Acetylation of histones is functionally linked to actively transcribed, open chromatin, with various acetylated residues associated with different regulatory mechanisms, such as enhancer and promoter activity, as well as chromatin organization (2, 43). We thus set to examine early gene expression changes associated with mutant-IDH1 induction by RNA-sequencing analysis. Overall, astrocytes induced to express mutant-IDH1 for 7 d, compared to cells not treated with doxycycline, showed mild changes in gene expression, with a slight preference for downregulation of expression (245 genes significantly down-regulated; 219 genes significantly up-regulated, Fig. 4*A*). Of note, the genes up-regulated by mutant-IDH1 were enriched for oncogenic pathways such as KRAS, MYC, and TNFa (Fig. 4*B*).

To gain insights into the genomic locations associated with loss of histone acetylation, we profiled the genomic patterns of three acetylation marks, H3K9ac, H3K27ac, and H4K16ac, following mutant-IDH1 induction, by Cut&Run analysis (46). Genome-wide analysis confirmed a reduction in coverage over acetylated regions following mutant-IDH1 induction for all three acetylation marks, in agreement with our CyTOF data, and a previous report (Fig. 4*C*) (31). Concordantly, ATAC-seq indicated an attenuation in chromatin accessibility upon mutant-IDH1 induction (Fig. 4*D*). Despite the global loss of H3K9ac, genes up-regulated by mutant-IDH1 showed slightly higher levels of H3K9ac at their promoters, in accordance with their increased expression (Fig. 4*E*). In control noninduced cells, these three acetylation sites on histone H3 and H4 were located both at promoter regions and at intronic and intergenic regions, in agreement with the literature (*SI Appendix*, Fig. S6*A*) (48–50). Thus, we explored which of these genomic features show the loss of histone acetylation. Interestingly, while we did not see changes in H3K9ac levels across all active transcription start sites (TSS), a significant reduction in H3K9ac signal was detected over enhancer regions, suggesting that the decrease in acetylation signal observed in our CyTOF analysis stems mainly from changes over intergenic regions (Fig. 4*F*) (47). These data support the notion that mutant-IDH1 alters acetylation patterns over distal genomic regions, which are known to comprise regulatory elements such as enhancers.

In contrast to H3K9ac, we observed a reduction in H3K27ac and H4K16ac signal over both active TSS and distal regions (Fig. 4*G* and *SI Appendix*, Fig. S6*B*). ATAC-seq revealed decreased chromatin accessibility over H3K27ac peaks upon induction of mutant-IDH1, supporting a functional role for the loss of H3K27ac in promoting a less accessible chromatin state in these regions (Fig. 4*H*). H3K27ac is considered a classical mark for active enhancers and is used to define super-enhancers, critical for cell-identity establishment and expression of oncogenic transcriptional programs (51–53). Interestingly, IDH1^{mut} cells showed a decrease in H3K27ac not only on regular enhancers but also on super-enhancers (Fig. 4*G*). To explore the functional consequences of these alterations to the enhancer landscape, we identified 229 super-enhancers unique to control cells (compared to cells expressing mutant-IDH1 for 7 d). Genes associated with these super-enhancers were enriched for terms related to cellular senescence and chromatin organization and were, in general, down-regulated upon mutant-IDH1 induction (Fig. 4*I*

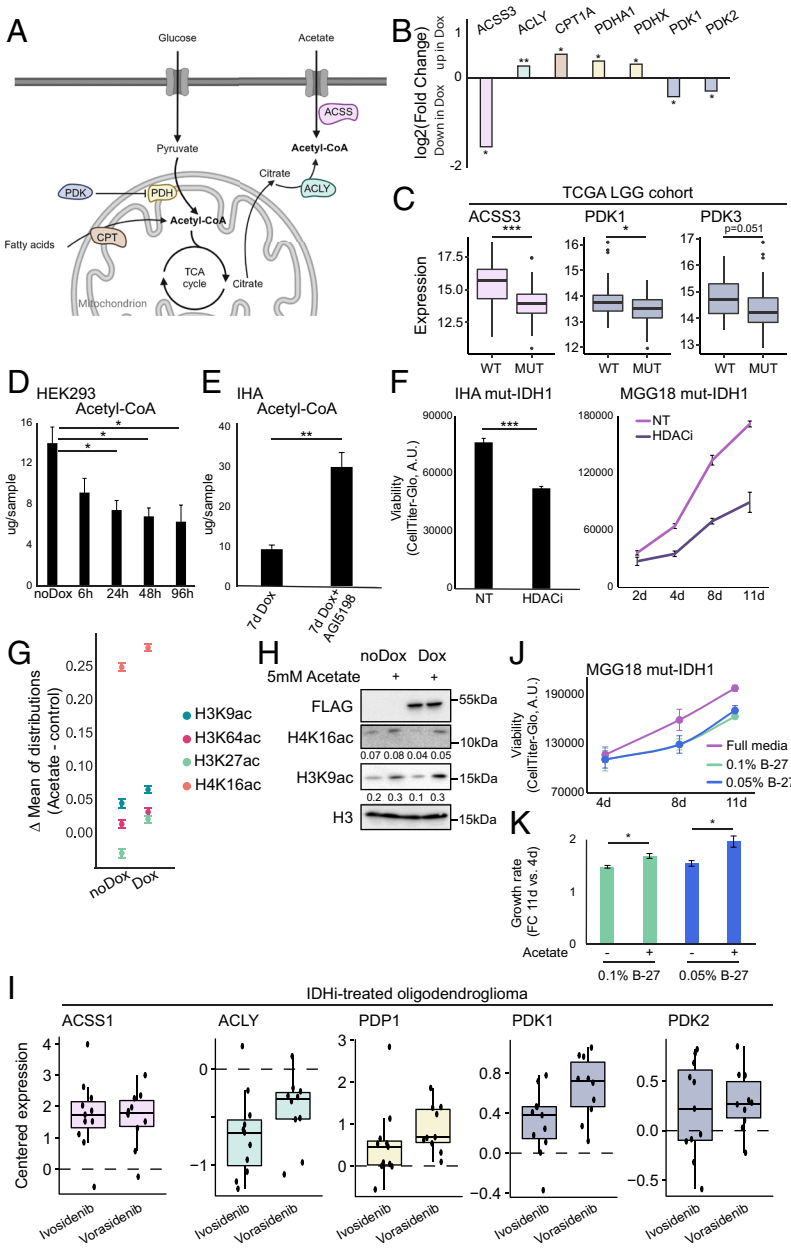

Fig. 3. Acetate supplement rescues histone acetylation and supports the growth of mutant-IDH1-expressing cells. (*A*) A simplified scheme of metabolic pathways, marked with different colors, associated with acetyl-CoA homeostasis. See *SI Appendix*, Table S3 for the full gene list. The illustration was created with BioRender.com and adapted from ref. 39. (*B*) Bar plot showing Log2 fold change of the indicated genes in IHA induced to express mutant-IDH1 (7 d). Shown are the genes from the list in *SI Appendix*, Table S3 that were significantly differentially expressed. **P*-value < 0.05, ***P*-value < 0.01. See also *SI Appendix*, Fig. S5*A*. (*C*) Expression levels of acetyl-CoA-related metabolic genes that significantly differ between WT (n = 34) and IDH1^{mut} (n = 91) low-grade gliomas (TCGA LGG cohort). Expression levels are shown as log2(fpkm − uq + 1); **P*-value < 0.05, ****P*-value < 0.001; two-sided *t* test with Benjamini–Hochberg correction for multiple testing. Box plots show center line as median, box limits as upper and lower quartiles, and whiskers extend from the edge to 1.5 * IQR. Data beyond the end of the whiskers are plotted individually as outlying points. (*D* and *E*) Quantification of cellular acetyl-CoA levels by LC–MS/MS in HEK293 cells expressing IDH1-R132H for the indicated time points (*D*), or IHA induced to express IDH1-R132H for 7 d and treated with 5 μM of AGI5198 for 5 d as in Fig. 2*C* (*E*). Mean ± SE of three biological (*D*) or technical (*E*) replicates are shown. **P*-value < 0.05, ***P*-value < 0.01; two-sided *t* test. Expression of mutant-IDH1 results in a decrease in acetyl-CoA levels. (*F*) Cell viability, as measured by CellTiterGlo, is shown for IHA treated with Dox and 1 μM Vorinostat for 72 h (*Left* panel) and MGG18 induced to express mutant IDH1 grown in low B-27 media (0.1%) and treated with 1 μM Vorinostat (*Right* panel). Media supplemented with Dox and HDACi was changed every 2 to 3 d. Mean ± SE of three technical repeats is shown. ****P*-value < 0.001; two-sided *t* test. (*G* and *H*) IHA were induced to express mutant-IDH1 for 4 d and supplemented with 5 mM acetate 2 d prior to collection for CyTOF (*G*) or western blot (*H*) analysis. (*G*) Mean differences between acetate and nontreated cells are shown for the indicated acetylation marks in cells induced to express mutant-IDH1 compared to control. Error bars represent SEM, calculated by bootstrapping. (*H*) Western blot analysis of the above-described samples, with the indicated antibodies. Signal intensity was normalized to H3 signal and indicated below each blot. Acetate supplement restores histone acetylation to higher levels in mutant-IDH1 expressing cells. Panel composition used for each experiment is described in *SI Appendix*, Table S2. (*I*) Expression levels of acetyl-CoA-related metabolic genes across 21 IDHi-treated oligodendroglioma bulk RNA-seq profiles from a perioperative phase 1 trial (NCT03343197). Samples are grouped by preoperative treatment regime. Scores are shown relative to the mean score of the two preoperatively untreated samples. Shown are only genes from the signature in *SI Appendix*, Table S3 that significantly differ between treated and untreated samples (*P*-value < 0.05, two-sided *t* test, Benjamini–Hochberg correction for multiple testing). Individual data points are shown in black ellipses. (*H*) MGG18 induced to express mutant-IDH1 were grown in either full media (2% B-27, v/v) or starved for acetate by reducing B-27 supplement concentration to 0.1% or 0.05% of original. Cell viability, as measured by CellTiterGlo, is shown at indicated timepoints. Mean ± SE of three technical repeats is shown. (*I*) MGG18 induced to express mutant-IDH1 were grown in low B-27 levels and supplemented with 5 mM acetate. For each condition, the growth rate was calculated as the fold of the CellTiter-Glo measurements on day 4 and day 11. Mean ± SE of three technical repeats is shown. **P*-value < 0.05; two-sided *t* test. Acetate supplement increases growth of MGG18 mutant-IDH1 cells.

and *SI Appendix*, Fig. S6*C*). Overall, our genome-wide analysis suggests that induction of mutant-IDH1 results in an altered enhancer landscape due to the widespread loss of histone acetylation marks. Interestingly, while changes in gene expression patterns were observed, they were mild at this early time point, perhaps reflecting the relatively long time it takes for these tumors to grow.

Mutant-IDH1 Increases Heterogeneity in Human and Mouse Glioma Cells and in Human Tumors. The high-dimensional single-cell data generated by the epigenetic CyTOF are not only limited to quantitative measurements of global alterations in each histone mark but can also teach us about the epigenetic diversity and heterogeneity within cells in the population. As the effect of mutant-IDH1 on histone acetylation marks may vary between different cells, we reasoned that this could result in a heterogeneous population. To explore this possibility, we performed dimensionality reduction by UMAP, using all measured features, and calculated the global distance between every two cells in the population, as defined by the 95th quantile of the distribution of distances between any two points in the population. If a population exhibits longer distances between cells, it suggests higher heterogeneity within this cell population. Interestingly, across all UMAP parameters, the induction of mutant-IDH1 in astrocytes gradually increased epigenetic heterogeneity (Fig. 5*A*). Furthermore, in the same sample, cells expressing higher levels of mutant-IDH1 showed greater heterogeneity (Fig. 5*B*). A similar increase was seen in the long-term mutant-IDH1 expressing MGG18 cells compared to the control cells, and in patient-derived HGG cells, harboring ATRX and TP53 inactivating mutations, stably expressing IDH1 R132H [Fig. 5 *C* and *D*, (54). Furthermore, inhibition of mutant-IDH1 with either AGI5198 or Vorasidenib (AG-881) in human or mouse mutant-IDH1-expressing cells resulted in lower epigenetic

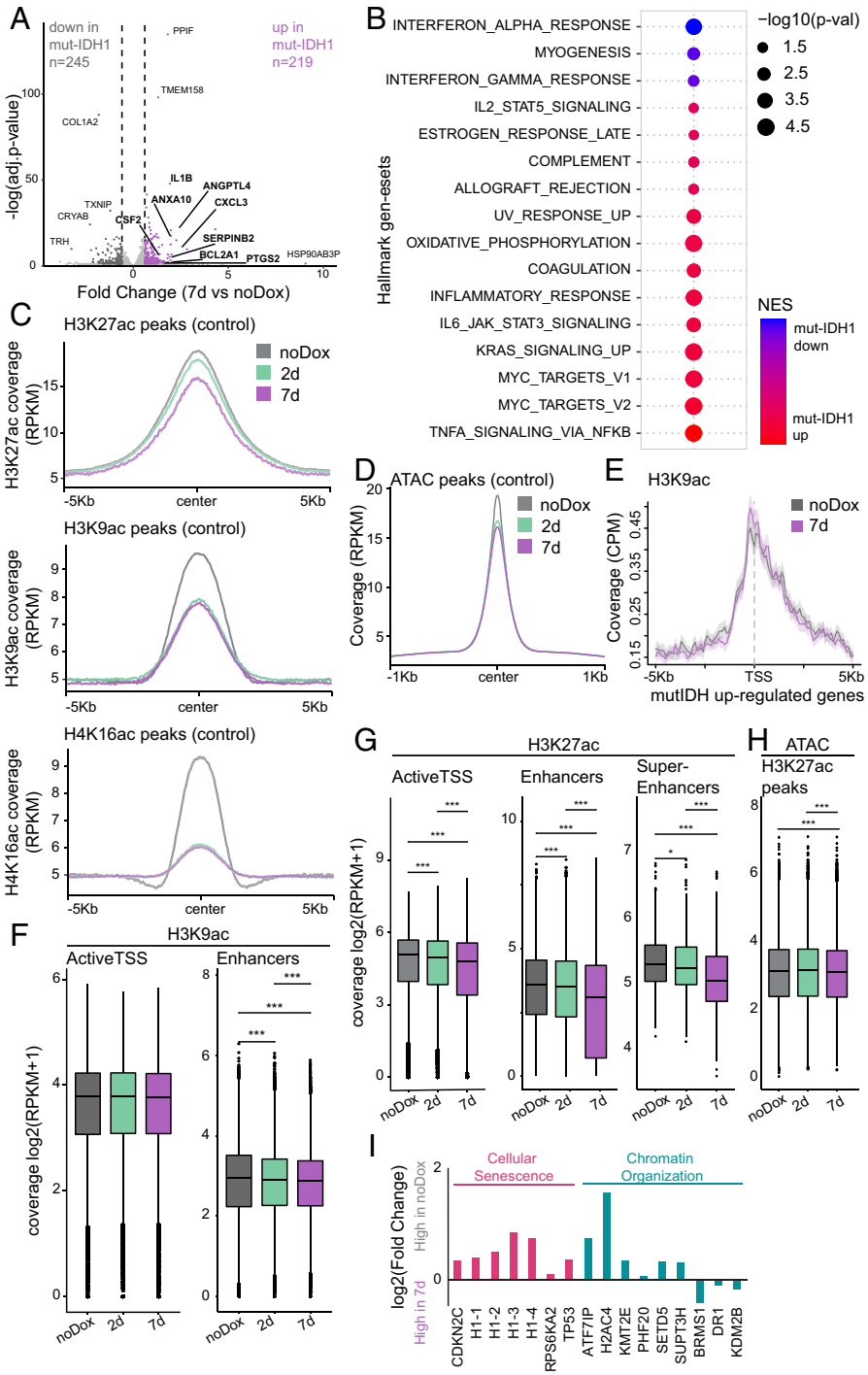

Fig. 4. Mutant-IDH1 promotes expression of oncogenic signatures and alters enhancer landscape. (*A*) Gene expression differences between IHA induced to express IDH1-R132H and control cells were plotted according to magnitude of change (log2FoldChange, *x*-axis) and significance (−log10(*P*.adj), *y*-axis). Dashed lines designate FC > 1.5. Gray and purple dots depict genes significantly deregulated (FC > 1.5, *P*.adj < 0.05). Genes depicted in bold contribute to the extreme leading edge of the enriched oncogenic gene sets shown in *B*. (*B*) Gene set enrichment analysis (GSEA) of expression differences between control and mutant-IDH1 expressing cells (7d). Genes were ranked according to fold change and compared to MSigDB Hallmark gene set (44, 45). Enriched signatures were ordered according to enrichment score; circle size corresponds to *P*-value of enrichment and the color to directionality; Red denotes terms enriched in genes up-regulated in mutant-IDH1 expressing cells. (*C*–*F*) IHA induced to express IDH1-R132H for 2 d and 7 d were analyzed by Cut&Run (46) for histone acetylation marks. (*C* and *D*) Average coverage of H3K27ac, H3K9ac, H4K16ac (*C*) and ATAC signal (*D*) over peaks identified in the control (no dox) IHA cells (H3K27ac peaks, n = 51,129; H3K9ac peaks, n = 84,938; H4K16ac, n = 103,983; ATAC-seq peaks n = 643,076). Acetylated signal, as well as chromatin accessibility, is reduced following mutant-IDH1 induction, in line with the CyTOF data. (*E*) Average coverage of H3K9ac over TSS of genes up-regulated in mutant-IDH1 cells (n = 219). Lines depict average coverage; shaded areas represent SE. (*F*) H3K9ac coverage on active TSS (n = 32,209) and enhancers (n = 110,036) in cells expressing mutant-IDH1 for the indicated times. Reduction in H3K9ac signal following mutant-IDH1 induction is seen over enhancers. For each genomic feature, mean coverage in each condition was calculated. Genomic annotation was derived from ChromoHMM analysis of IHA (47). ***P-value < 0.001. (*G*) H3K7ac coverage on active TSS (n = 32,209), enhancers (n = 110,035), and super-enhancers (n = 993, *Methods Summary*), plotted as in *D*. *P-value < 0.05, ***P-value < 0.001. H3K27ac signal is significantly reduced on regulatory elements following mutant-IDH1 induction. (*H*) ATAC-seq coverage over H3K27ac peaks identified by Cut&Run analysis in noninduced IHA (n = 51,129 peaks). ***P-value < 0.001. Chromatin accessibility is reduced in H3K27ac marked regions upon induction of mutant-IDH1. (*I*) Bar plot showing Log2 fold change of the indicated genes in IHA induced to express mutant-IDH1 (7 d). Shown genes are related to functional terms, associated with super-enhancers unique to the control cells that do not express mutant-IDH1 (*SI Appendix*, Fig. S6*C*). *P*-values were calculated by the pairwise *t* test, with Bonferroni correction for multiple comparisons.

heterogeneity (Fig. 5 *E* and *F*). These results suggest a robust role for mutant-IDH1 in affecting epigenetic heterogeneity in diverse cellular contexts.

To explore a different measure of heterogeneity, we calculated for each modification the Gini coefficient, commonly used to measure the inequality among the values of a frequency distribution; so that higher values indicate higher diversity (55). Most chromatin marks scored higher Gini index in mutant-IDH1 expressing cells than control cells, supporting increased epigenetic heterogeneity (Fig. 5 *G* and *H*). Interestingly, acetylation marks were among the marks which showed the highest increase in heterogeneity, further highlighting the functional link between these marks and mutant-IDH1. Concordantly, inhibition of the mutant protein resulted in a lower Gini index of several modifications, including the four acetylation marks measured (Fig. 5*I*). These data indicate that expression of mutant-IDH1 leads to increased epigenetic diversity between cells in multiple histone modifications, resulting in increased epigenetic heterogeneity in the population of cells.

Finally, we aimed to explore whether the effect of mutant-IDH1 on epigenetic heterogeneity has functional consequences for transcriptional heterogeneity in human IDH^{mut} oligodendroglioma patients. To that end, we leveraged a recently published single-cell transcriptomic profiling of a matched pair of samples taken from an individual diagnosed with grade 2 oligodendroglioma, pretreatment, and 4 wk after initiation of IDH inhibition (34). Importantly, we found that inhibiting mutant-IDH in this patient led to reduced transcriptional heterogeneity, as measured by the

mean distance between cells in each sample and the distribution of the global distances between each two cells in the pre- and posttreatment samples (Fig. 5*J*). Moreover, the decrease in transcriptional heterogeneity following mutant-IDH inhibition was also seen when comparing global distance scores in single-cell transcriptomic samples from six nontreated oligodendroglioma patients compared to two individuals treated with IDH inhibitors (Fig. 5*K* and *SI Appendix*, Fig. S7) (34, 41, 42). While limited to a small number of tumors, our analysis suggests a chromatin-based mechanism that may contribute to the high transcriptional heterogeneity found in glioma and may be reversed, at least partially, by mutant IDH inhibitors

Discussion

Epigenetic reprogramming has been suggested as a driver of gliomagenesis (7). For IDH^{mut} tumors, this has been supported by the low mutational burden and the highly altered metabolic state of these tumors (35, 56). The effects of mutant-IDH on chromatin patterns have been studied mainly within the context of inhibition of demethylation enzymes by the 2-HG oncometabolite (18, 28, 29). Here, we aimed to apply an unbiased approach to study the early epigenetic events mediated by introduction of this mutant enzyme in nontransformed astrocytes, as IDH1 mutations are thought to occur early in glioma development. Thus, we applied high-dimensional single-cell analysis to profile a wide array of histone modifications following short induction of IDH1-R132H in astrocytes. We find that global reduction in multiple histone acetylation marks is an early consequence of mutant-IDH1 expression, observed across diverse biological systems. Of note, expression of R172K IDH2 in mouse cells was shown to result in a decrease in H3 acetylation, as detected by a pan Ac-H3 antibody, suggesting that this loss of histone acetylation may also be associated with mutations in IDH2 (18). Importantly, this loss was not observed in astrocytes treated with 2-HG, in line with previous metabolic profiling, showing both common and unique alterations between mutant-IDH and 2-HG (22). Nevertheless, high levels of 2-HG may contribute partially to reduction in histone acetylation marks, since we did observe lower levels of H4K16ac in 2-HG treated cells. In the context of neuronal stem cells, 2-HG have been shown to reduce acetyl-CoA levels, causing the reduction in H3K27ac and chromatin accessibility observed in D2HGDH deficient cells (57). Yet, the degree and cellular consequences of 2-HG accumulation following IDH1 expression and D2HGDH downregulation differ substantially and seem to be highly cell-type dependent.

The hypermethylated phenotype of mutant-IDH1 cells has been associated with impaired chromatin accessibility, blocking differentiation (20). Furthermore, a recent study by Schvartzman and colleagues linked the increase in heterochromatin with impaired DNA replication and replication stress (56). Our study highlights that inhibition of αKG-dependent demethylases may not be the sole mechanism by which mutant-IDH1 promotes heterochromatin formation. Loss of acetylation on histone residues can facilitate chromatin compaction and thus increase heterochromatin (58). Indeed, our ATAC-seq analysis revealed that enhancers that lost H3K27ac upon expression of mutant-IDH1 showed reduced accessibility. Importantly, the loss of histone acetylation occurs immediately following mutant-IDH1 induction and therefore is probably not a result of changes in cellular growth rates or indirect downstream alterations.

We provide evidence for rewiring of acetyl-CoA-related metabolic pathways by mutant-IDH1 in several model systems and in human tumors. Interestingly, multiple pathways regulating acetyl-CoA availability are affected, some of which are context-dependent and may exert opposing effects on acetyl-CoA levels. For example, downregulation of PDK and ACSS family members is expected to reduce acetyl-CoA, while upregulation of ACLY and CPT1A may increase it. These results, seen in both the IHA experimental system and in patients, emphasize IDH1-mediated rewiring of acetyl-CoA metabolism. Expression of IDH^{mut} alters the balance between the different pathways, which regulates the levels of this important metabolite in different cellular compartments and from different sources (39, 59). In addition, CPT1A and CPT1C are affected differently by mutant-IDH1, depending on the cells examined, highlighting context-specific variation in mutant-IDH1-dependent metabolic rewiring. Further studies are needed to explore the direct consequences of alteration in each pathway to acetyl-CoA levels in different cellular compartments, in the context of glioma cells.

Overall, this metabolic rewiring leads to changes in the availability of acetate derivatives, and specifically acetyl-CoA, thus affecting chromatin maintenance. Upon external addition of such metabolites, IDH1^{mut} cells can restore histone acetylation levels, suggesting that the molecular machinery of deposition is intact. Acetylation of histones may serve as reservoirs of acetyl groups, which can be transferred to activating acetylation sites upon specific stimuli (24, 36, 60). The metabolic rewiring of IDH1^{mut} cells may require the depletion of such nuclear reservoirs of acetyl groups for nuclear or cytoplasmic use. Of note, this may point toward a metabolic vulnerability of cells expressing the mutant enzyme. Indeed, IDH inhibition reverted the expression changes of acetyl-coA-related metabolic genes in oligodendroglioma patients. Moreover, the growth of IDH1-mutant cells under starvation was enhanced by addition of acetate, pointing to a potential metabolic dependency. In line with this observation, a recent study by Garrett et al. suggests HDAC1 and HDAC6 as potential drug-targetable enzymes supporting growth in IDH1 mutant gliomas (31). Inhibition of HDAC enzymes may deplete mutant-IDH1 cells of the needed acetyl groups that are normally removed from histone storage sites, thus compromising viability. Of note, our genome-wide analysis revealed reduced acetylation marks mainly in intergenic regions, which may serve as such storage sites. Nevertheless, we observed changes in enhancer landscape following mutant-IDH1 induction, contributing to the gene expression differences detected. Thus, it is likely that loss of acetylation on chromatin, mediated by mutant-IDH1 expression, may affect both enhancer activity and potential "storage" sites, eventually contributing to deregulated epigenetic landscapes and glioma development. Of note, despite the global loss of histone acetylation, there are genes that are transcriptionally up-regulated upon mutant-IDH1 induction. These genes not only maintain H3K9ac levels, but show slightly higher levels at their promoters, supporting the notion that histone acetylation loss can be regulated in a loci-specific manner. It is possible that these up-regulated genes gain activating histone methylation marks, such as H3K4me3, following induction of IDH^{mut}, preventing loss of histone acetylation and consequently leading to their increased expression. Importantly, some of these genes are implicated in oncogenic pathways, such as KRAS, MYC, and TNFα, potentially contributing to the oncogenic properties of mutant-IDH1.

Our CyTOF approach provides a framework for analyzing multiple marks in a highly quantitative and sensitive manner. The single-cell resolution allows for the analysis of heterogeneity in the cellular response. While we see a global reduction in acetylation, it seems highly heterogeneous between cells. Increased heterogeneity was also observed for the histone methylation marks in IDH1-mutant-expressing cells. This suggests that each cell responds differently to the metabolic challenge, rendering it harder

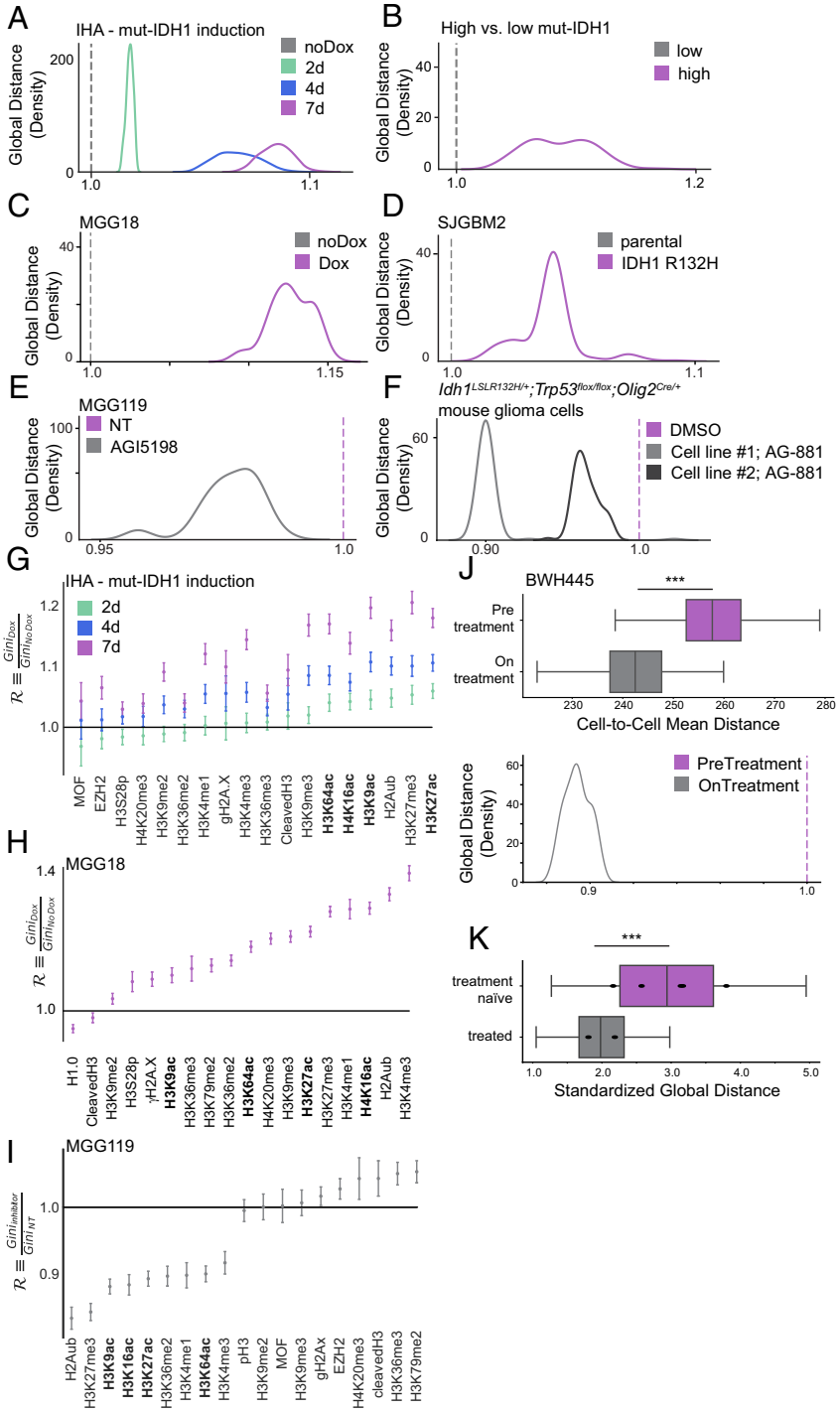

Fig. 5. Expression of mutant-IDH1 contributes to higher epigenetic heterogeneity. (*A* and *B*) IHA induced to express IDH1-R132H for 2, 4, and 7 d were analyzed by CyTOF. Joint UMAP was performed for all samples and the global distance between each two cells in each sample was calculated across a wide range of UMAP parameters. (*A*) Plotted are the ratios of the values of each induction time point; values over 1 indicate excess heterogeneity following mutant-IDH1 induction. (*B*) Within the cell population treated with doxycycline for 7 d cells were divided by mutant-IDH1 expression levels (as defined by FLAG signal). Comparison of epigenetic heterogeneity was conducted as described in *A*. (*C*) MGG18 cells expressing IDH1-R132H compared to noninduced cells were analyzed as in *A*. (*D*) Patient-derived HGG cells, transfected and selected for stable expression of IDH1 R132H, compared to parental cells (WT-IDH1), were analyzed as in *A*. Expression of mutant-IDH1 increases epigenetic heterogeneity. (*E* and *F*) Human MGG119 cells (endogenously expressing *IDH1*^{R132H}) treated with 5 μM AGI5198 (*E*) and two pairs of mouse glioma cells endogenously expressing mutant *Idh1* (*Idh1*$^{LSL\text{-}R132H}$;*Trp53*$^{flox/flox}$;*Olig2*^{Cre}) treated with 1 μM AG-881 (*F*), compared to control cells, were analyzed as in *A*. Inhibition of mutant-IDH1 lowers epigenetic heterogeneity. (*G–I*) The Gini coefficient was used to determine the relative heterogeneity of each chromatin-related marker between the different samples. The ratio of the Gini coefficient between IHA (*G*) or MGG18 (*H*) induced to express mutant-IDH1 versus control samples is shown as a measure of the excess heterogeneity. (*I*) The ratio of the Gini coefficient between MGG119 cells treated with the IDH inhibitor AGI5198 versus control cells. (*J–K*) Single-cell RNAseq data of pre- and on-treatment samples (*J*) and treatment naïve compared to treated oligodendrogliomas (*K*) was analyzed to evaluate transcriptional heterogeneity (34). (*J*) *Upper* panel: bootstrapped mean cell-to-cell distance. The pairwise Euclidean distance between 500 single cells, randomly selected without replacement from each population, was calculated and repeated 500 times. ***P-value < 0.001, two-sided t test. *Bottom* panel: the distribution of the global distances between each two cells in each sample (as the analysis shown in panels *A–F*). (*K*) From each tumor, 100 malignant cells were randomly selected without replacement (samples with less than 100 informative malignant cells were not included). TPM values were z-scored, and the global distance between cells in each tumor was calculated as in panels *A–F*. Boxplots groups tumors according to treatment status (treatment naïve, n = 5; treated, n = 2). The mean global distance score for each tumor is shown as individual data points. ***P-value < 0.001, two-sided t test. See *SI Appendix*, Fig. S7 for the distribution of each tumor. CyTOF panel composition used for each experiment is described in *SI Appendix*, Table S2.

to detect robust chromatin and transcriptional changes. An interesting speculation would be that this increased heterogeneity may provide the population of IDH1-mutant cells a greater fitness advantage or enhance their ability to adapt to diverse and changing environmental conditions. Indeed, treatment of mutant-IDH1 mouse glioma cells with the IDH inhibitor Vorasidenib, recently tested in the phase 3 INDIGO clinical (33), resulted in an increase in histone acetylation marks and reduced epigenetic heterogeneity. Importantly, single-cell transcriptomics analysis of patients treated with IDH inhibitor revealed a reduction in transcriptional heterogeneity following the treatment. These results further support a role for mutant-IDH1 in mediating epigenetic heterogeneity, with consequences for transcriptional heterogeneity. Overall, this study highlights the tight interaction between metabolic rewiring and chromatin dynamics in cancer cells and underscores the power of single-cell epigenetic analysis.

Methods Summary

Cell Culture. IHA, fetal-SV40, were obtained from abm. MGG18 cells transduced with doxycycline-dependent IDH1-R132H were generated in Prof. Daniel Cahill`s laboratory (61).

Mouse glioma cells (NRAS^{G12V}, p53 KD, ATRX KD with or without IDH1-R132H) were generated in Prof. Maria Castro's laboratory (54). Mouse glioma cells (*Idh1*$^{LSL\text{-}R132H}$;*Trp53*$^{flox/flox}$;*Olig2*^{Cre}) were generated in Dr. Jerome Fortin's laboratory (32).

Antibody Metal Conjugation and CyTOF Analysis. Antibodies were conjugated to metals using the MIBItag Conjugation Kit (IONpath), according to the manufacturer's protocols. Sample preparation and CyTOF analysis were conducted as described in ref. 27. All antibodies are listed in *SI Appendix*, Table S1.

Expression Analysis of Human Tumor Samples. Xena browser (62) was used to visualize expression data from the TCGA LGG cohort. Samples tested for IDH1 mutation were included (n = 125).

Expression data from phase 1 IDHi trial (NCT03343197) were analyzed as described in refs. 34 and 40. As indicated by Spitzer et al. (34), patients at Massachusetts General Hospital (MGH) were consented preoperatively in all cases according to Institutional Review Board DF/HCC 10-417. All human data/samples were deidentified prior to use.

Single-cell RNA-seq data of nontreated and IDHi-treated oligodendrogliomas were downloaded and analyzed as described in ref. 34.

Data, Materials, and Software Availability. All sequencing data are deposited in NCBI's Gene Expression Omnibus (GEO) under Accession No. GSE238106 (63). CyTOF fcs files are deposited in Flow Repository (FR-FCM-Z6LF) (64). CyTOF epigenetic analysis is available at https://doi.org/10.5281/zenodo.8178524 (65).

ACKNOWLEDGMENTS. We thank H. Keren-Shaul, R. Blecher-Gonen, Y. Elazari, N. Adler-Berke, I. Bolocan-Nachman, and R. Ronen from the Crown Genomics Institute of the Nancy and Stephen Grand Israel National Center for Personalized Medicine, Weizmann Institute of Science, for their help with NGS experiments. We thank N. Harpaz for her help in designing the CyTOF experiments and D. Cahill for generously providing the MGG18-IDH1-R132H cultures. E.S. is an incumbent of the Lisa and Jeffrey Aronin Family Career Development chair and is also supported by Henry Chanoch Krenter Institute for Biomedical Imaging and Genomics. This research was supported by grants from the European Research Council (ERC101115455), The Israel Science Foundation (1881/19 and 1349/24), Emerson Collective, The Israel Cancer Research Fund, the German-Israeli Cooperation in Cancer Research and Minerva.

Author affiliations: [a]Department of Immunology and Regenerative Biology, Weizmann Institute of Science, Rehovot 7610001, Israel; [b]Department of Molecular Cell Biology, Weizmann Institute of Science, Rehovot 7610001, Israel; [c]Oncology Institute, Tel Aviv Sourasky Medical Center, Tel Aviv 6423906, Israel; [d]Faculty of Medicine, Tel Aviv University, Tel Aviv 6997801, Israel; [e]Mass Cytometry Unit, Life Sciences Core Facilities, Weizmann Institute of Science, Rehovot 7610001, Israel; [f]Bioinformatics Unit, Department of Life Sciences Core Facilities, Faculty of Biochemistry, Weizmann Institute of Science, Rehovot 7610001, Israel; [g]Targeted Metabolomics Unit, Life Sciences Core Facilities, Weizmann Institute of Science, Rehovot 7610001, Israel; [h]The Institute for Drug Research, Faculty of Medicine, Hebrew University, Jerusalem 9112102, Israel; [i]Sagol School of Neurobiology, Department of Biochemistry and Molecular Biology, The George S. Wise Faculty of Life Sciences, Tel Aviv University, Tel Aviv 6997801, Israel; [j]Department of Neurosurgery, University of Michigan Medical School, Ann Arbor, MI 48109; [k]Department of Neurology and Neurosurgery, Montreal Neurological Institute-Hospital, McGill University, Montreal, QC H3A 2B4, Canada; [l]Department of Pathology and Center for Cancer Research, Massachusetts General Hospital and Harvard Medical School, Boston, MA 02114; [m]Broad Institute of Harvard and MIT, Cambridge, MA 02142; and [n]Racah Institute of Physics, Hebrew University, Jerusalem 9190401, Israel

Author contributions: N.F., G.R., and E.S. designed the research; N.F., N.C., T.-M.S., T.M., and A.B. performed experiments; A.S., A.M., D.F.-M., M.G.C., J.F., M.L.S., I.T., and A.E. contributed new reagents/analytic tools and provided invaluable suggestions; N.F., A.S., B.D., I.T., G.R., and E.S. analyzed data; and N.F. and E.S. wrote the paper.

1. C. M. Rivera, B. Ren, Mapping human epigenomes. *Cell* **155**, 39–55 (2013).
2. T. Kouzarides, Chromatin modifications and their function. *Cell* **128**, 693–705 (2007).
3. P. Chi, C. D. Allis, G. G. Wang, Covalent histone modifications–Miswritten, misinterpreted and mis-erased in human cancers. *Nat. Rev. Cancer* **10**, 457–469 (2010).
4. W. A. Flavahan, E. Gaskell, B. E. Bernstein, Epigenetic plasticity and the hallmarks of cancer. *Science* **357**, eaal2380 (2017).
5. D. Hanahan, Hallmarks of cancer: New dimensions. *Cancer Discov.* **12**, 31–46 (2022).
6. P. A. Jones, J. P. Issa, S. Baylin, Targeting the cancer epigenome for therapy. *Nat. Rev. Genet.* **17**, 630–641 (2016).
7. R. E. Phillips, A. A. Soshnev, C. D. Allis, Epigenomic reprogramming as a driver of malignant glioma. *Cancer Cell* **38**, 647–660 (2020), 10.1016/j.ccell.2020.08.008.
8. D. N. Louis *et al.*, The 2021 WHO classification of tumors of the central nervous system: A summary. *Neuro Oncol.* **23**, 1231–1251 (2021).
9. H. Yan *et al.*, IDH1 and IDH2 mutations in gliomas. *N. Engl. J. Med.* **360**, 765–773 (2009).
10. J. Rees *et al.*, Volumes and growth rates of untreated adult low-grade gliomas indicate risk of early malignant transformation. *Eur. J. Radiol.* **72**, 54–64 (2009).
11. M. Tanguy, Continuous growth of mean tumor diameter in a subset of grade II gliomas. *Ann. Neurol.* **53**, 524–528 (2003).
12. D. W. Parsons *et al.*, An integrated genomic analysis of human glioblastoma multiforme. *Science* **321**, 1807–1812 (2008).
13. T. Watanabe, S. Nobusawa, P. Kleihues, H. Ohgaki, IDH1 mutations are early events in the development of astrocytomas and oligodendrogliomas. *Am. J. Pathol.* **174**, 1149–1153 (2009).
14. Z. J. Reitman, H. Yan, Isocitrate dehydrogenase 1 and 2 mutations in cancer: Alterations at a crossroads of cellular metabolism. *J. Natl. Cancer Inst.* **102**, 932–941 (2010).
15. L. Dang *et al.*, Cancer-associated IDH1 mutations produce 2-hydroxyglutarate. *Nature* **462**, 739–744 (2009).
16. P. S. Ward *et al.*, The common feature of leukemia-associated IDH1 and IDH2 mutations is a neomorphic enzyme activity converting α-ketoglutarate to 2-hydroxyglutarate. *Cancer Cell* **17**, 225–234 (2010).
17. W. Xu *et al.*, Oncometabolite 2-hydroxyglutarate is a competitive inhibitor of α-ketoglutarate-dependent dioxygenases. *Cancer Cell* **19**, 17–30 (2011).
18. C. Lu *et al.*, IDH mutation impairs histone demethylation and results in a block to cell differentiation. *Nature* **483**, 474–478 (2012).
19. W. A. Flavahan *et al.*, Insulator dysfunction and oncogene activation in IDH mutant gliomas. *Nature* **529**, 110–114 (2016).
20. J.-M. Schvartzman, V. P. Reuter, R. P. Koche, C. B. Thompson, 2-hydroxyglutarate inhibits MyoD-mediated differentiation by preventing H3K9 demethylation. *Proc. Natl. Acad. Sci. U.S.A.* **116**, 12851–12856 (2019).
21. S. Han *et al.*, IDH mutation in glioma: Molecular mechanisms and potential therapeutic targets. *Br. J. Cancer* **122**, 1580–1589 (2020).
22. Z. J. Reitman *et al.*, Profiling the effects of isocitrate dehydrogenase 1 and 2 mutations on the cellular metabolome. *Proc. Natl. Acad. Sci. U.S.A.* **108**, 3270–3275 (2011).
23. M. Garrett *et al.*, Metabolic characterization of isocitrate dehydrogenase (IDH) mutant and IDH wildtype gliomaspheres uncovers cell type-specific vulnerabilities. *Cancer Metab.* **6**, 4 (2018).
24. W.-C. Hsieh *et al.*, Glucose starvation induces a switch in the histone acetylome for activation of gluconeogenic and fat metabolism genes. *Mol. Cell* **82**, 60–74.e65 (2022).
25. C. Pessoa Rodrigues *et al.*, Histone H4 lysine 16 acetylation controls central carbon metabolism and diet-induced obesity in mice. *Nat. Commun.* **12**, 6212 (2021).
26. C. Chung *et al.*, Integrated metabolic and epigenomic reprograming by H3K27M mutations in diffuse intrinsic pontine gliomas. *Cancer Cell* **38**, 334–349.e339 (2020).
27. N. Harpaz *et al.*, Single-cell epigenetic analysis reveals principles of chromatin states in H3.3-K27M gliomas. *Mol. Cell* **82**, 2696–2713.e2699 (2022).
28. S. Turcan *et al.*, Mutant-IDH1-dependent chromatin state reprogramming, reversibility, and persistence. *Nat. Genetics* **50**, 62–72 (2018).
29. S. Turcan *et al.*, IDH1 mutation is sufficient to establish the glioma hypermethylator phenotype. *Nature* **483**, 479–483 (2012).
30. S. Doll, A. Urisman, J. A. Oses-Prieto, D. Arnott, A. L. Burlingame, Quantitative proteomics reveals fundamental regulatory differences in oncogenic HRAS and isocitrate dehydrogenase (IDH1) driven astrocytoma. *Mol. Cell Proteomics* **16**, 39–56 (2017).
31. M. C. Garrett *et al.*, HDAC1 and HDAC6 are essential for driving growth in IDH1 mutant glioma. *Sci. Rep.* **13**, 12433 (2023).
32. E. Laugesen *et al.*, MODL-47 in a new mouse model of IDH mutated gliomas identifies tumor cells of origin and determinants of sensitivity to IDH inhibitors. *Neuro-Oncology* **25**, v309 (2023).
33. I. K. Mellinghoff *et al.*, Vorasidenib in IDH1- or IDH2-mutant low-grade glioma. *N. Engl. J. Med.* **389**, 589–601 (2023).
34. A. Spitzer *et al.*, Mutant IDH inhibitors induce lineage differentiation in IDH-mutant oligodendroglioma. *Cancer Cell* **42**, 904–914.e909 (2024).
35. I. C. Hvinden, T. Cadoux-Hudson, C. J. Schofield, J. S. O. McCullagh, Metabolic adaptations in cancers expressing isocitrate dehydrogenase mutations. *Cell Rep. Med.* **2**, 100469 (2021).
36. M. Mendoza *et al.*, Enzymatic transfer of acetate on histones from lysine reservoir sites to lysine activating sites. *Sci. Adv.* **8**, eabj5688 (2022).
37. P. Mews *et al.*, Alcohol metabolism contributes to brain histone acetylation. *Nature* **574**, 717–721 (2019).
38. K. E. Wellen *et al.*, ATP-citrate lyase links cellular metabolism to histone acetylation. *Science* **324**, 1076–1080 (2009).
39. X. Bian *et al.*, Lipid metabolism and cancer. *J. Exp. Med.* **218**, 784 (2020).
40. I. K. Mellinghoff *et al.*, Vorasidenib and ivosidenib in IDH1-mutant low-grade glioma: A randomized, perioperative phase 1 trial. *Nat. Med.* **29**, 615–622 (2023).
41. I. Tirosh *et al.*, Single-cell RNA-seq supports a developmental hierarchy in human oligodendroglioma. *Nature* **539**, 309–313 (2016).
42. A. S. Venteicher *et al.*, Decoupling genetics, lineages, and microenvironment in IDH-mutant gliomas by single-cell RNA-seq. *Science* **355**, eaai8478 (2017).
43. M. Shvedunova, A. Akhtar, Modulation of cellular processes by histone and non-histone protein acetylation. *Nat. Rev Mol. Cell Biol.* **23**, 329–349 (2022).
44. A. Subramanian *et al.*, Gene set enrichment analysis: A knowledge-based approach for interpreting genome-wide expression profiles. *Proc. Natl. Acad. Sci. U.S.A.* **102**, 15545–15550 (2005).
45. A. Liberzon *et al.*, The molecular signatures database (MSigDB) hallmark gene set collection. *Cell Syst.* **1**, 417–425 (2015).
46. P. J. Skene, S. Henikoff, An efficient targeted nuclease strategy for high-resolution mapping of DNA binding sites. *eLife* **6**, e21856 (2017).
47. A. Kundaje *et al.*, Integrative analysis of 111 reference human epigenomes. *Nature* **518**, 317–330 (2015).
48. K. Karmodiya, A. R. Krebs, M. Oulad-Abdelghani, H. Kimura, L. Tora, H3K9 and H3K14 acetylation co-occur at many gene regulatory elements, while H3K14ac marks a subset of inactive inducible promoters in mouse embryonic stem cells. *BMC Genomics* **13**, 424 (2012).
49. A. Radzisheuskaya *et al.*, Complex-dependent histone acetyltransferase activity of KAT8 determines its role in transcription and cellular homeostasis. *Mol. Cell* **81**, 1749–1765.e1748 (2021).
50. M. P. Creyghton *et al.*, Histone H3K27ac separates active from poised enhancers and predicts developmental state. *Proc. Natl. Acad. Sci. U.S.A.* **107**, 21931–21936 (2010).
51. D. Hnisz *et al.*, Super-enhancers in the control of cell identity and disease. *Cell* **155**, 934–947 (2013).
52. J. Lovén *et al.*, Selective inhibition of tumor oncogenes by disruption of super-enhancers. *Cell* **153**, 320–334 (2013).

53. S. Sengupta, R. E. George, Super-enhancer-driven transcriptional dependencies in cancer. *Trends Cancer* **3**, 269–281 (2017).
54. F. J. Núñez *et al.*, IDH1-R132H acts as a tumor suppressor in glioma via epigenetic up-regulation of the DNA damage response. *Sci. Transl. Med.* **11**, eaaq1427 (2019).
55. C. Gini, *On the Measure of Concentration with Special Reference to Income and Wealth* (Cowles Commission, 1936), vol. 2.
56. J.-M. Schvartzman *et al.*, Oncogenic IDH mutations increase heterochromatin-related replication stress without impacting homologous recombination. *Mol. Cell* **83**, 2347–2356.e8 (2023).
57. Y. Liu, M. Wang, Y. Guo, L. Wang, W. Guo, D-2-hydroxyglutarate dehydrogenase governs adult neural stem cell activation and promotes histone acetylation via ATP-citrate lyase. *Cell Rep.* **42**, 112067 (2023).
58. L. T. Bailey, S. J. Northall, T. Schalch, Breakers and amplifiers in chromatin circuitry: Acetylation and ubiquitination control the heterochromatin machinery. *Curr. Opin. Struct. Biol.* **71**, 156–163 (2021).
59. F. Pietrocola *et al.*, Acetyl coenzyme A: A central metabolite and second messenger. *Cell Metab.* **21**, 805–821 (2015).
60. C. Ye, B. P. Tu, Sink into the epigenome: Histones as repositories that influence cellular metabolism. *Trends Endocrinol. Metab.* **29**, 626–637 (2018).
61. K. Tateishi *et al.*, Extreme vulnerability of IDH1 mutant cancers to NAD+ depletion. *Cancer Cell* **28**, 773–784 (2015).
62. M. J. Goldman *et al.*, Visualizing and interpreting cancer genomics data via the Xena platform. *Nat. Biotechnol.* **38**, 675–678 (2020).
63. N. Furth *et al.*, High-dimensional analysis reveals increased chromatin heterogeneity and reduced histone acetylation driven by mutant-IDH1. Gene Expression Omnibus (GEO). https://www.ncbi.nlm.nih.gov/geo/query/acc.cgi?acc=GSE238106. Deposited 24 July 2023.
64. N. Furth *et al.*, CyTOF fcs files from Oncogenic IDH1mut drives robust loss of histone acetylation and increases chromatin heterogeneity. Flow. http://flowrepository.org/id/FR-FCM-Z6LF. Deposited 24 July 2023.
65. N Furth *et al.*, Code for CyTOF epigenetic analysis. Zenodo. https://zenodo.org/records/8178524. Deposited 24 July 2023.